Stochastic Dipolar Recoupling in Nuclear Magnetic Resonance of Solids

Robert Tycko*

Laboratory of Chemical Physics, National Institute of Diabetes and Digestive and Kidney Diseases, National Institutes of Health, Bethesda, Maryland 20892-0520, USA

(Received 1 August 2007; published 2 November 2007)

I describe a nuclear magnetic resonance (NMR) technique, called stochastic dipolar recoupling (SDR), that permits continuous experimental control of the character of spin dynamics between coherent and incoherent limits in a system of magnetic dipole-coupled nuclei. In the fully incoherent limit of SDR, spin polarization transfers occur at distance-dependent rates without the quantum mechanical interferences among pairwise dipole-dipole couplings that often limit the feasibility or precision of structural studies of solids by NMR. In addition to facilitating structural studies, SDR represents a possible route to experimental studies of effects of decoherence on the dynamics of quantum many-body systems.

DOI: 10.1103/PhysRevLett.99.187601 PACS numbers: 76.60.Pc, 33.15.Bh, 61.18.Fs, 87.15.−v

The inverse cubic dependence of magnetic dipole-dipole couplings on internuclear distances is the basis for many structural studies of solids by nuclear magnetic resonance (NMR). In two-spin systems, accurate distances are readily obtained from dipole-dipole couplings [1–3]. However, in many-spin systems, quantum mechanical interference among noncommuting pairwise dipole-dipole couplings leads to complicated coherent spin dynamics, and hence NMR data that do not depend simply on pairwise distances. The data depend on the full geometry of the spin system [3,4], and longer distances can not be determined quantitatively in the presence of shorter distances. Here I introduce an approach to measurements of dipole-dipole couplings, called stochastic dipolar recoupling (SDR), that permits experimental control of the spin dynamics between fully coherent and fully incoherent limits. In the incoherent limit, quantum mechanical interference is eliminated and the dynamics are accurately described by pairwise rates of polarization transfers among coupled spins, proportional to the inverse sixth power of pairwise distances. SDR therefore provides a new basis for structural investigations of solids by NMR. In addition, continuous control of the balance between coherent and incoherent processes through an experimental parameter ($f_{\max}$, defined below) is a novel aspect of SDR with potential implications for fields outside NMR, including macroscopic quantum tunneling [5] and quantum information processing [6], where techniques analogous to SDR may be used to investigate effects of decoherence on quantum algorithms [7].

High resolution and high sensitivity in NMR of solids require rapid sample rotation about the "magic angle" $\theta_m = \cos^{-1}\frac{1}{\sqrt{3}}$ relative to the external static magnetic field. Magic-angle spinning (MAS) averages dipole-dipole couplings to zero, but radio-frequency (rf) pulse sequences applied in synchrony with MAS, called dipolar recoupling sequences [2,8–10], create nonzero average dipole-dipole couplings. The recoupled dipole-dipole Hamiltonian for like nuclei with gyromagnetic ratio γ has the form $H_D = \sum_{i>j} d_{ij} A_{ij}$, with coupling constants $d_{ij} = \hbar\gamma^2/R_{ij}^3$ for internuclear distances, R_{ij}. In general, $[A_{ij}, A_{ik}] \neq 0$ for $j \neq k$, causing stronger couplings to truncate (i.e., suppress the effects of) weaker couplings in coherent evolution under H_D.

Figure 1 shows the pulse sequence used in SDR experiments. After ^{1}H-^{13}C cross polarization [11], an optional t_1 evolution period for two-dimensional (2D) spectroscopy, and a 90° pulse to convert transverse ^{13}C spin polarization to longitudinal spin polarization, the SDR sequence is applied. This consists of alternating periods of double-quantum (DQ) recoupling [12,13] and free evolution under isotropic chemical shifts (CS), lasting $n\tau_R$ and $m\tau_R$, where τ_R is the MAS rotation period. During DQ periods, the spin Hamiltonian is $H_{\mathrm{DQ}} = \sum_{i>j} d_{ij}[g_{ij}(\Omega) I_{+i} I_{+j} + g_{ij}(\Omega)^* I_{-i} I_{-j}]$, where g_{ij} is a function of the molecular orientation Ω in the MAS rotor [13] and $I_{\pm i}$ are angular momentum raising and lowering operators for spin i. During the kth CS period, the Hamiltonian is

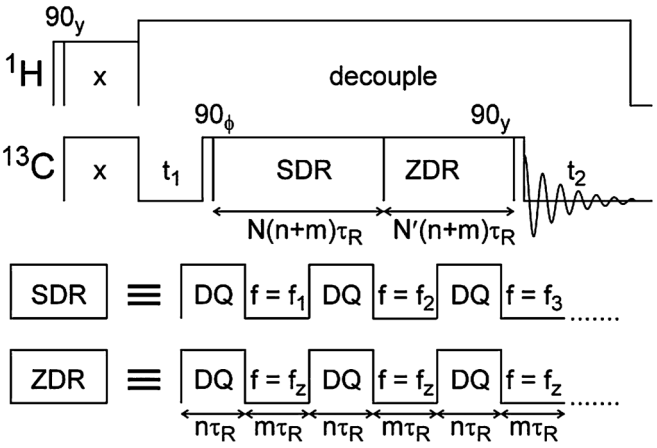

FIG. 1. Radio-frequency pulse sequence for SDR in ^{13}C NMR of solids.

$H_{CS}^{(k)} = \sum_i (\delta_i + f_k) I_{zi}$, where δ_i is the chemical shift of spin i and f_k is an rf carrier frequency offset, chosen randomly in the interval $[-f_{max}, f_{max}]$. In an interaction representation with respect to H_{CS}, no evolution takes place during CS periods, and evolution during the kth DQ period occurs under the transformed Hamiltonian $\tilde{H}_{DQ}^{(k)} = \sum_{i>j} d_{ij}[g_{ij}(\Omega) e^{i\Phi_{ij}(k)} I_{+i} I_{+j} + g_{ij}(\Omega)^* e^{-i\Phi_{ij}(k)} I_{-i} I_{-j}]$, with $\Phi_{ij}(k) = \sum_{q=1}^{k-1} m(\delta_i + \delta_j + 2f_q)\tau_R$ for $k > 1$ and $\Phi_{ij}(1) = 0$. Thus, pairwise couplings are phase-modulated according to the $\Phi_{ij}(k)$ values (which become random variables when $f_{max} \neq 0$), leading to the incoherent spin dynamics demonstrated below.

In Fig. 1, the SDR period is followed by a period of ''zero dipolar recoupling'' (ZDR) in which the carrier offsets are fixed at a value f_z that is chosen to average H_{DQ} coherently to zero for the given set of chemical shifts [14]. Inclusion of the ZDR period permits ''constant-time'' experiments, in which $(N + N')(m + n)\tau_R$ is kept constant while the net recoupling time $Nn\tau_R$ is varied, thus minimizing effects of spin relaxation and pulse imperfections [3]. A 90° pulse after the ZDR period excites ^{13}C free-induction decay (FID) signals, which are detected in the t_2 period.

Experiments were performed in a 9.4 T magnetic field (100.4 MHz ^{13}C NMR frequency) using a Varian InfinityPlus spectrometer and 3.2 mm MAS probe. The POST-C7 sequence of Hohwy *et al.* [13] was used in DQ periods, implemented as a train of 56 90° pulses of length $\tau_R/28 - t_{ps}$ separated by phase-switching delays $t_{ps} = 0.30\ \mu s$, with $\tau_R = 134.23\ \mu s$ (7.450 kHz MAS frequency) and $n = 2$. ^1H decoupling field amplitudes were 130 kHz. Values of f_k were calculated with a random number algorithm within the pulse program, producing different values for each FID, except that the same f_k values were used to acquire real and imaginary t_1 data ($\phi = y$ and $\phi = x$ in Fig. 1) in 2D experiments. Three powder samples were examined, with isotopic dilution to reduce intermolecular couplings: L-alanine, with 5% of molecules labeled at C_α and C_β sites ($^{13}C_2$-ALA); sodium bisulfite adduct of acetone, with 5% of molecules labeled at both methyl sites ($^{13}C_2$-BSA); β-D-ribofuranose tetraacetate powder, with 9% of molecules labeled at the five ribose sites ($^{13}C_5$-RFTA). ^{13}C carrier frequencies corresponding to $f_k = 0$ were at the midpoint of the C_α and C_β lines for $^{13}C_2$-ALA, on-resonance with the methyl line for $^{13}C_2$-BSA, and near the center of the five ribose lines for $^{13}C_5$-RFTA.

Figure 2 shows experimental data for $^{13}C_2$-ALA and $^{13}C_2$-BSA. With $f_{max} = 0$, the ^{13}C NMR signals (sum of C_α and C_β peak areas for $^{13}C_2$-ALA in Fig. 2(a); methyl peak area for $^{13}C_2$-BSA in Fig. 2(b)] have oscillatory dependences on $Nn\tau_R$, reflecting coherent quantum mechanical evolution under H_{DQ}. The ratio of oscillation periods (15.0 ms/3.48 ms = 4.31) is nearly equal to the cube of the ratio of intramolecular internuclear distances

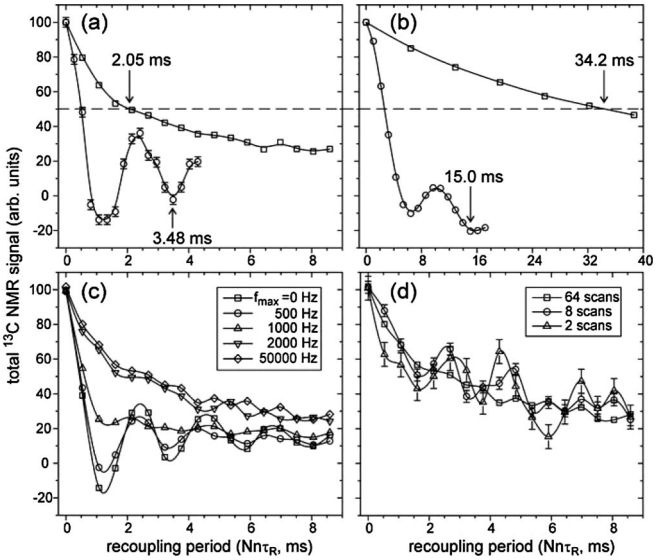

FIG. 2. SDR in two-spin systems. (a) NMR signal amplitude from $^{13}C_2$-ALA as a function of the dipolar recoupling time $Nn\tau_R$, using the pulse sequence in Fig. 1 with $f_{max} = 0$ Hz (circles) or 10^5 Hz (squares) and with $n = 2$, $m = 1$, $N + N' = 16$ (circles) or 32 (squares), $f_z = 2300$ Hz, and 16 (circles) or 128 (squares) scans per data point. A constant natural-abundance ^{13}C signal was subtracted, determined from the known ratio of labeled to unlabeled molecules. Lines are guides to the eye. (b) Same for $^{13}C_2$-BSA, but with $N + N' = 64$ (circles) or 128 (squares), $f_z = 2200$ Hz, and 128 scans per data point. (c) Dependence of signals from $^{13}C_2$-ALA on f_{max}, with $N + N' = 32$, 64 scans per data point, and other conditions identical to panel a. (d) Dependence of signals from $^{13}C_2$-ALA on the number of scans per data point, with $f_{max} = 5 \times 10^4$ Hz and other conditions identical to panel (c). Error bars are uncertainties determined from the root-mean-squared noise in the ^{13}C NMR spectra.

[2] [(0.251 nm/0.154 nm)^3 = 4.33], as expected for coherent evolution. With $f_{max} = 10^5$ Hz, the signals decay in a monotonic manner. The ratio of 50% decay times (34.2 ms/2.05 ms = 16.7) is nearly equal to the sixth power of the ratio of internuclear distances [(0.251 nm/0.154 nm)^6 = 18.7], suggesting incoherent evolution determined by rates that depend on the squares of couplings. Figure 2(c) shows the progression from coherent to incoherent limits, controlled by the pulse sequence parameter f_{max}. Figure 2(d) shows that smooth, monotonic signal decay at large f_{max} emerges only after averaging over the random f_k values. When only 2 or 8 scans are averaged for each data point, deviations from monotonic decay are significantly greater than uncertainties due to noise.

SDR data for a two-spin system depend on f_{max} through the quantity $\sin\theta_{max}/\theta_{max}$, with $\theta_{max} = 4\pi m f_{max} \tau_R$. SDR data could be acquired equivalently by applying random rf phase shifts to successive DQ blocks while keeping the carrier frequency in CS periods constant.

Figure 3(a) shows results of numerical simulations with conditions that mimic those in Fig. 2(a). Agreement with

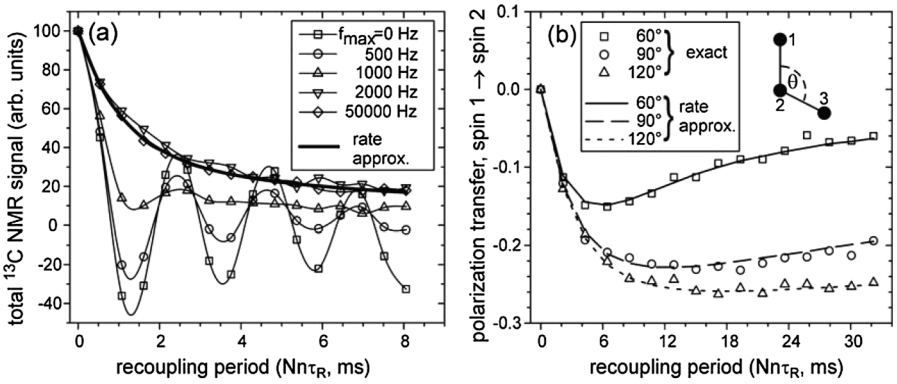

FIG. 3. Simulations of SDR in ^{13}C NMR. Powder averages over 1728 orientations were performed, with different random choices of f_k for each orientation and with $n = 2$, $m = 1$, and $N' = 0$, (a) Two-spin system with 0.157 nm separation. Light lines are guides to the eye. Heavy line is a rate approximation simulation described in the text. (b) Three-spin system with 0.200 nm separations between spins 1 and 2 and spins 2 and 3. The amplitude of spin polarization transfer from spin 1 to spin 2 was calculated as a function of the angle θ using either a full quantum mechanical simulation with $f_{\max} = 10^5$ Hz (squares, circles, triangles) or the rate approximation (solid, long dashed, short dashed lines). The three spins have NMR frequencies of 2000, 500, and -2000 Hz relative to the carrier frequency at $f_k = 0$.

experimental data is excellent apart from more rapid damping of oscillations in the experimental data at small values of $f_{\max}$ (due to spin relaxation effects that are not included in the simulations). The heavy solid line in Fig. 3(a) is a ''rate approximation'' simulation, in which evolution of longitudinal spin polarization during the recoupling period is assumed to consist of polarization transfers that are determined by a rate matrix $\mathbf{W}$ with off-diagonal elements $W_{ij} = -\sin^2|nd_{ij}g_{ij}(\Omega)\tau_R|$ and diagonal elements $W_{jj} = 1 + \sum_{i\neq j} W_{ij}$, where $g_{ij}(\Omega)$ is extracted from a numerical calculation of the propagator $U_{\mathrm{DQ}} \equiv \exp(-inH_{\mathrm{DQ}}\tau_R)$. If longitudinal polarizations in an M-spin system at $t = 0$ are represented by an M-dimensional vector $\mathbf{p}_0$, then polarizations at $t = Nn\tau_R$ are $\mathbf{p}_N = \mathbf{W}^N\mathbf{p}_0$. The rate approximation simulation in Fig. 3(a) agrees well with full quantum mechanical simulations for large $f_{\max}$, indicating that coherences can be neglected after each DQ period. The rate approximation is accurate when $|nd_{ij}g_{ij}(\Omega)\tau_R| \ll 1$ for all spin pairs, implying that $W_{ij} \approx -|ng_{ij}(\Omega)\tau_R\hbar\gamma^2|^2/R_{ij}{}^6$.

Figure 3(b) shows full quantum mechanical and rate approximation simulations for a three-spin system with several hypothetical geometries. Again, the rate approximation agrees well with the full quantum mechanical treatment for large $f_{\max}$, even though the rate approximation ignores quantum mechanical effects due to noncommutivity of pairwise couplings. The good agreement indicates that correlations among $\Phi_{ij}(k)$ values for different spin pairs in $\tilde{H}^{(k)}_{\mathrm{DQ}}$ are negligible, provided that $\delta_i + \delta_j$ is different for each pair.

Figure 4(b) shows experimental 2D ^{13}C-^{13}C NMR spectra of $^{13}C_5$-RFTA for several values of $Nn\tau_R$, with $f_{\max} = 5 \times 10^4$ Hz. Strong cross peaks arising from nearest-neighbor polarization transfers during the recoupling period are observed at $Nn\tau_R = 2.148$ ms. Cross peaks corresponding to non-nearest-neighbor polarization transfers increase in amplitude with increasing $Nn\tau_R$. Figure 4(c) compares experimental amplitudes for polarization transfers t_{ij} between spins i and j (measured as cross peak volumes) with rate approximation simulations based on the known molecular structure [Fig. 4(a)] [15], either including all rate matrix elements in the five-spin system or including only elements W_{ij} with $|i - j| = 1$ (i.e., only nearest-neighbor rates). Simulated amplitudes are scaled to minimize the total squared deviation s^2 from experimental amplitudes, with the same scaling factor for all $Nn\tau_R$ values. Both simulations reproduce the signs and approximately the relative amplitudes of the experimental data. However, $s^2 = 0.0241$ when all rates are included, while $s^2 = 0.0399$ when only nearest-neighbor rates are included. For full quantum mechanical simulations (not shown), $s^2 = 0.0239$, indistinguishable from the rate approximation. These observations suggest that the experimental cross peaks in Fig. 4(b) do not result only from sequential nearest-neighbor polarization transfers, but instead result from both sequential nearest-neighbor and direct non-nearest-neighbor transfers.

Discrepancies between experimental and simulated t_{ij} values in Fig. 4(c) at small $Nn\tau_R$ values are largely due to imperfect suppression of polarization transfers during the ZDR period.

Experimental data and simulations presented above support the utility of SDR as a structural tool with potential applications to inorganic, organic, and biological materials [16–18]. SDR data in NMR of solids closely resemble nuclear Overhauser effect data that are commonly used to determine molecular structures in NMR of liquids [19], but the random modulations of dipole-dipole couplings in SDR are under experimental control rather than being a result of thermal motions. Additional theoretical aspects of SDR are presented elsewhere [20].

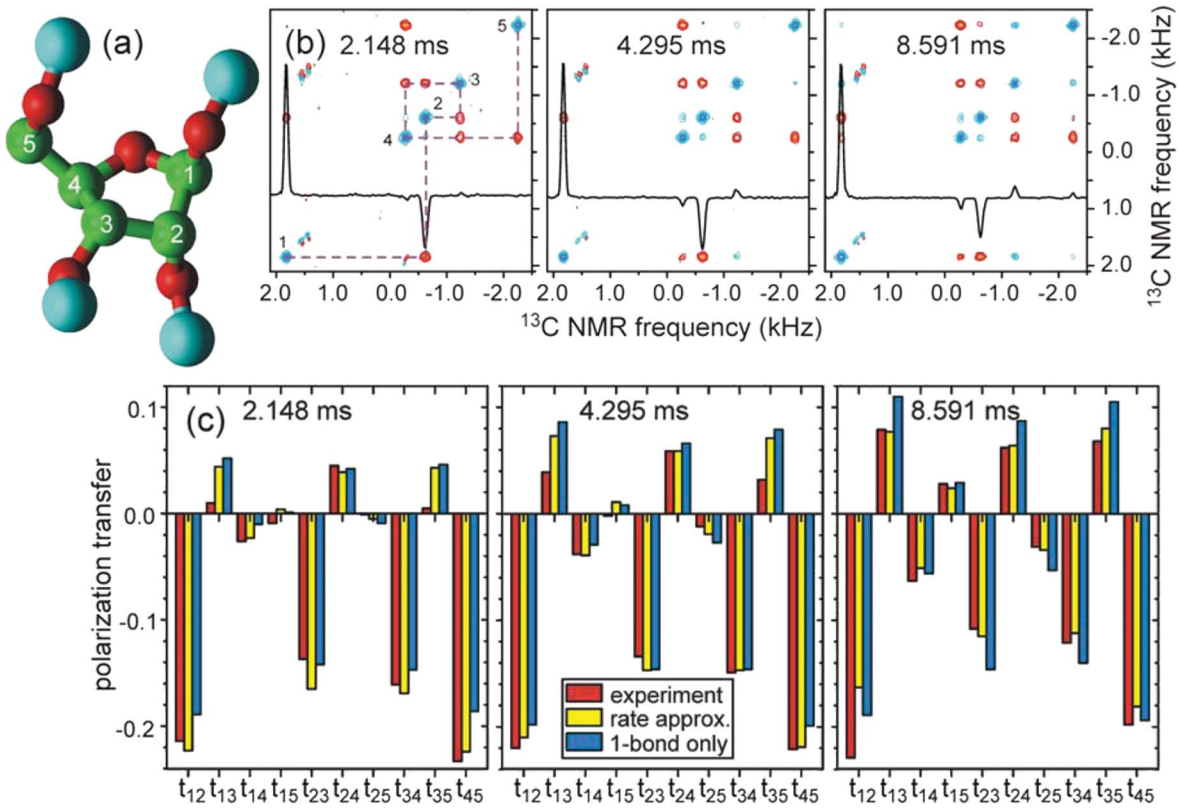

FIG. 4 (color). SDR in a five-spin system. (a) Molecular model of RFTA, showing ^{13}C-labeled sites (green), oxygen atoms (red), and acetyl groups (blue); (b) 2D NMR spectra at the indicated values of $Nn\tau_R$. Positive and negative contour levels are blue and red, increase by successive factors of two, and are the same in all three spectra. Frequency scale is relative to the rf carrier at $f_k = 0$. 1D slices through the NMR line of site 1 are shown. Spectra were obtained with 25 complex t_1 points, a 193.2 μs t_1 increment, 64 scans per t_1 point, $f_z = 1800$ Hz, $m = 2$, $n = 2$, and $N + N' = 32$. (c) Experimental polarization transfer amplitudes (red bars), with t_{ij} being the average of volumes for the ij and ji crosspeaks, and rate approximation calculations, including either all dipole-dipole couplings (yellow bars) or only nearest-neighbor couplings (blue bars).

This work was supported by the Intramural Research Program of the National Institute of Diabetes and Digestive and Kidney Diseases and the Intramural AIDS Targeted Antiviral Program of the National Institutes of Health. $^{13}C_5$-RFTA was synthesized from $^{13}C_5$-ribose by Dr. Wai-Ming Yau.

*robertty@mail.nih.gov

[1] G. E. Pake, J. Chem. Phys. **16**, 327 (1948).
[2] R. Tycko and G. Dabbagh, Chem. Phys. Lett. **173**, 461 (1990).
[3] R. Tycko, J. Chem. Phys. **126**, 064506 (2007).
[4] S. Kiihne, M. A. Mehta, J. A. Stringer, D. M. Gregory, J. C. Shiels, and G. P. Drobny, J. Phys. Chem. A **102**, 2274 (1998).
[5] Y. Yu, S. Y. Han, X. Chu, S. I. Chu, and Z. Wang, Science **296**, 889 (2002).
[6] D. Jaksch, J. I. Cirac, P. Zoller, S. L. Rolston, R. Cote, and M. D. Lukin, Phys. Rev. Lett. **85**, 2208 (2000).
[7] D. A. Lidar, I. L. Chuang, and K. B. Whaley, Phys. Rev. Lett. **81**, 2594 (1998).
[8] B. H. Meier and W. L. Earl, J. Am. Chem. Soc. **109**, 7937 (1987).
[9] R. Tycko, Phys. Rev. Lett. **60**, 2734 (1988).
[10] T. Gullion and J. Schaefer, J. Magn. Reson. **81**, 196 (1989).
[11] A. Pines, M. G. Gibby, and J. S. Waugh, J. Chem. Phys. **59**, 569 (1973).
[12] W. S. Warren, S. Sinton, D. P. Weitekamp, and A. Pines, Phys. Rev. Lett. **43**, 1791 (1979).
[13] M. Hohwy, H. J. Jakobsen, M. Eden, M. H. Levitt, and N. C. Nielsen, J. Chem. Phys. **108**, 2686 (1998).
[14] A. K. Paravastu and R. Tycko, J. Chem. Phys. **124**, 194303 (2006).
[15] P. Bombicz, M. Czugler, R. Tellgren, and A. Kalman, Angew. Chem., Int. Ed. **42**, 1957 (2003).
[16] D. H. Brouwer, R. J. Darton, R. E. Morris, and M. H. Levitt, J. Am. Chem. Soc. **127**, 10365 (2005).
[17] B. Elena and L. Emsley, J. Am. Chem. Soc. **127**, 9140 (2005).
[18] C. Ritter, M. L. Maddelein, A. B. Siemer, T. Luhrs, M. Ernst, B. H. Meier, S. J. Saupe, and R. Riek, Nature (London) **435**, 844 (2005).
[19] A. Kumar, G. Wagner, R. R. Ernst, and K. Wuthrich, J. Am. Chem. Soc. **103**, 3654 (1981).
[20] R. Tycko, J. Phys. Chem. B (to be published).